

3.3 COHERENT MICROSCALE SURFACE STRUCTURES OBSERVED BY A SCANNING LIDAR AND THEIR CONTRIBUTION TO MASS EXCHANGE IN THE STABLE BOUNDARY LAYER

D.I. Cooper^{*1}, W.E. Eichinger², M.Y. Leclerc³, J. Archuleta¹, C.Y.J. Kao¹

1. Los Alamos National Laboratory, Los Alamos, NM 87545

2. University of Iowa, Iowa City, IA 52242

3. University of Georgia, Griffin, GA 30223

1. INTRODUCTION

The application of high resolution scanning lidars to characterize the spatial properties of coherent microscale structures is well documented (Cooper et al., 1992, 1994, 1996, 1997, 2000). The Raman water vapor scanning lidar was used to examine selected spatial characteristics within the first 100 m of the atmosphere above the surface during a typical nocturnal regime. The three-dimensional atmospheric water vapor field over wheat stubble field on a gentle slope on the south-western edge of the Salt Lake City Basin in October of 2000 during the Vertical Mixing and Transport Experiment (VTMX) was mapped. In this paper, the detailed structure of the atmosphere, including low-frequency, intermittent, coherent structures will be shown to be intimately involved in the exchange of mass and energy between the surface and the atmosphere (Cooper et al., 2004).

Microscale coherent structures both observed and simulated within the stable boundary layer invokes the question: By what mechanism do such structures arise, and what mechanisms are responsible for their development? To address these questions, high temporal and spatial resolution properties of the surface-atmosphere interface is examined.

2. STUDY SITE

This study was part of an inter-institutional intensive sub-site headed by PNNL (called Site 11, as described in Doran et al., 2002) at the foot of the Oquirrh Mountains at 40.5394° North latitude, 112.0235° West longitude, about 11 km East of the Kennecott copper mine, and 3 km North of Herriman in the southern part of the Salt Lake City basin in Utah. The surface was

composed of bare soil and wheat stubble, approximately 20 cm tall on a gentle 1.58° east-facing slope, with a fetch in excess of 6 km (Fig. 1).

This experimental deployment took place in October 2000, where the nocturnal boundary layer included clear night inversions, and weak winds at height (Doran et al., 2002). This paper focuses upon a specific set of nocturnal observations that occurred during VTMX; that of clear skies and light winds at the surface and aloft, such as was found during the evening and morning of October 8th and 9th. Surface winds during the campaign were from the west, moving down-slope with drainage winds at 3 to 5 ms⁻¹ between 5 and 10 m above ground level (AGL). Surface level winds resulted from drainage flow, which was a dominant factor in surface-atmosphere exchange, in contrast with larger scale circulations. Inversions and drainage flows during the intensive operating period (IOP) began after sunset and was maintained throughout the evening until mid-morning. The temperature inversion was approximately 5 to 6 degrees deep at between 20 and 25 m AGL, as a result of a combination of clear-sky radiative cooling and surface thermal properties.

3. METEOROLOGICAL OBSERVATIONS

Four tether sondes were operated simultaneously with crews coordinated by D. Whiteman of PNNL. There ascents took place every 30 minutes using all four tether sondes, recording the usual variables of time, height, air pressure, air temperature, relative humidity, wind direction, and mean wind every 1 to 2 m, at intervals of about 3 s to a height of approximately 200 m.

The sonic anemometer collected u , v , w , and T_v at 10 Hz during VTMX on a tower at a height of 9.1 m AGL or 1475.1 m MSL. The sonic anemometer was approximately 11 km east of the Kennecott copper mine pit, and was 2.9 km on the 35° radial from Herriman, Utah, and about 3.5 km east of the lidar. The boom direction was 273° magnetically sighted from back to front along the boom.

3.1 Lidars

The lidar was located at 1539 m MSL, 300 m east of the PNNL tether sonde 4 site shown in Figure 1. Details on the method and operation of the scanning lidar are described in Eichinger et al. (1998). The absolute accuracy of the lidar was shown to be $\pm 0.34 \text{ gkg}^{-1}$ at the 95% confidence level (Eichinger et al. 1994). The LANL Raman lidar generated volume images from two-dimensional scans of range-resolved water vapor. The lidar azimuthal scan range covered 60° from North to South. The vertical scan range was from the surface up to

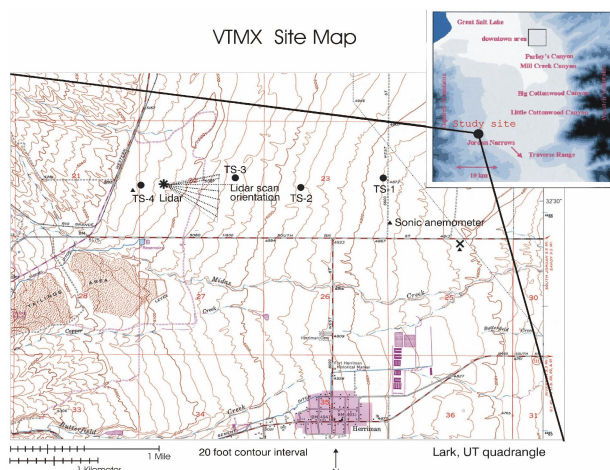


Figure 1. Study site map.

50 m into the SBL, and acquired lines-of-sight just south of the TS-3 site by approximately 5 m (Fig. 1). Horizontal transects or spatial-series, parallel to the surface were extracted from the vertical scans by averaging portions of several lines-of-sight together that comprised the region of interest. The lidar was operated to a radial range of about 600 m, a horizontal spatial resolution of 1.5 m. The azimuthal scanning range was up to 60°, and a vertical step resolution as small as 0.05°. Each vertical range-height scan required 52 s to complete, a set of 60 lines-of-sight stepped in 0.2° increments from -3° in elevation to 9° made up an individual range-height scan. The lidar was also used as a profiler with a minimum height of 50 m, and 1.5 m spatial resolution up to 600 m into the atmosphere.

The elastic lidar used in this experiment is a miniaturized vertical profiling system that uses a Nd:YAG laser at 1.064 μm to measure the relative backscatter intensity of micron sized or larger particles. It was mounted on the back of the Raman lidar trailer and collected data concurrently with the Raman lidar, at 100 Hz, and averaging together 1000 laser pulses for every line-of-sight to 10 s. The elastic lidar has a vertical resolution of 3 m and with a minimum range-bin of 100 m. The time-averaging procedure generated range-height time-series up to approximately 1000 m over a period of 90 minutes. Images compiled from the elastic backscatter data, while only qualitative in concentration are ideal to identify the time, height, and relative intensity of wave structures in the atmosphere above the first 100 m.

4. STABLE BOUNDARY LAYER STRUCTURES OBSERVED BY LIDAR

At the time of the elastic lidar vertical time-height scans shown in Fig. 2, structures are observed in the lower 700 m, with a moderate density region in the first 200 m, suggesting a possible boundary layer at approximately 600 m (Fig. 2). From 75 m to approximately 600 m, the relative backscatter intensity was approximately 66% lower than the solitary structure between 600 m and 700 m. This suggests that the lower

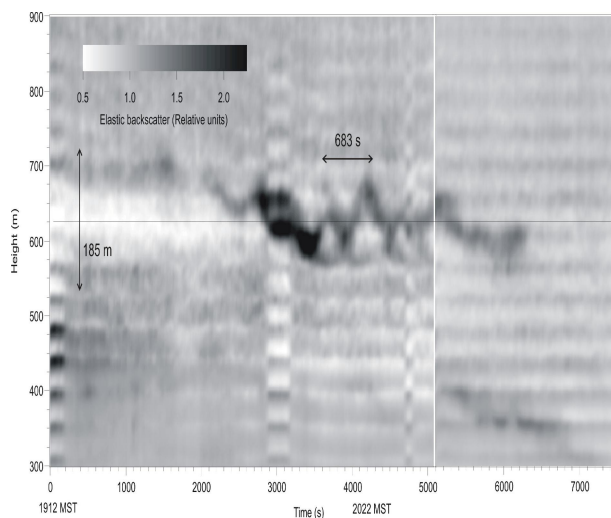


Figure 2. Elastic lidar time-height scan

part of the atmosphere was well mixed and relatively aerosol free. However, the relatively strong backscatter between 600 m and 700 m appears to define a “wave” about 30 minutes before the observed surface structures, and continues throughout the period when surface intermittency appears.

4.1 Raman Range-Height Vertical Scans

Nocturnal boundary layer microscale structures is seen in Fig. 3, which shows the intermittent low-frequency coherent structures responsible for much of the mass exchange between the surface and the atmosphere (Fig. 3). In this image, two structures are clearly connected with the surface, one at 325 m with a height of about 12 m and the larger geyser-like feature at 370 m, approximately 20 m high. Since these plumes are more humid than the background environment, it is expected that these structures are rising by buoyancy, dynamics, or a combination of both since the density of moist air is lower than dry air. In the absence of warming, the clear sky SBL will cool radiatively, resulting in the decay of the SBL depth. The life cycle for these coherent features in the range-height scans appears to be relatively short when compared to their analogues in daytime convective conditions (Cooper et al., 2003, Kao et al., 2002). From a time-series of sequential vertical spatial scans, it appears that individual coherent plume events are part of a series of turbulent “bursts” lasting less than 10 scans, or under 540 s from initiation to quiescence. For the most part, these microscale coherent structures do not penetrate the capping inversion as they do in convective conditions, and appear to rise to the capping inversion level and then, relatively quickly, fall back to the surface.

It appears that the transport and exchange of mass and energy between the surface and the atmosphere is limited to the first few tens of meters under the modest wind conditions observed. The main transport mechanism is by low-frequency, intermittent, coherent structures, and not by uniform diffusive vertical movement. In order to determine whether these microscale structures are local, attributed to micro-

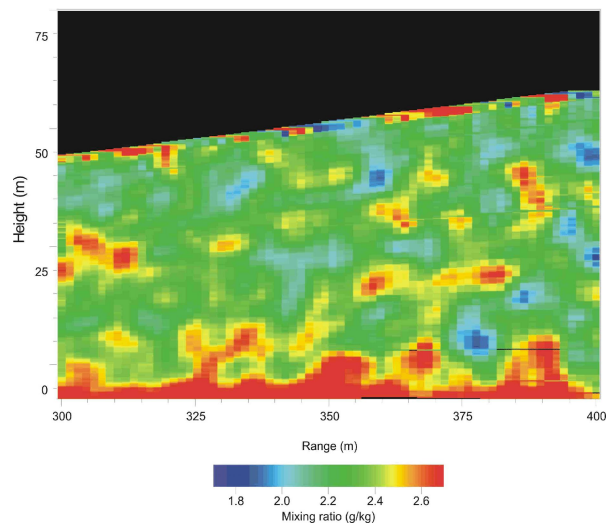


Figure 3. Raman lidar range-height scan.

topographical features or a drainage ditch, horizontal (range-range) scans were used to show whether or not these structures are found elsewhere at the site. A horizontal scan will determine whether the structures are localized, as these show up as moist spots in only one region of the image.

5. PERIODIC INTERMITTENCY

In the SBL, a mechanism was recently proposed to explain the development and decay of low frequency intermittency observed by both lidars or by point sensors (Rees et al., 1998; Sun et al., 2004) in terms of wave-turbulence interactions. Wave-turbulence interactions in the SBL were studied in detail in the eighties and nineties (Chimonas, 1993, 1999; Einaudi and Finnigan, 1981, 1993; Finnigan and Einaudi, 1981; Finnigan et al., 1984; Finnigan, 1988) and continues into the present (Cuxart et al., 2002; Mahrt and Vickers, 2002; Staquet and Sommeria, 2002). Mahrt (1999) suggested that in some stability regimes, the stable boundary layer is non-traditional, or “upside-down” in that the source of the turbulence is from elevated regions, generated from low level jets or gravity waves. The criteria for non-traditional stable boundary layers is that the downward heat flux is not a function of z/L . The data from the sonic anemometer showed no clear relationship between $-\overline{w'\theta_v'}$ and z/L , supporting the concept that the VTMX atmosphere fits into the non-traditional boundary layer regime. In a pioneering experimental study of the thermally stratified Antarctic boundary layer, Rees et al. (1998) proposed that near-surface organized structures observed using sonic anemometers within the first 32 m of the surface result from coupling of solitary waves aloft. The wave propagates down to the surface and interacts with the atmosphere within the near-surface waveguide, the interaction is by aerodynamic drag creating eddies and roll vortices in the SBL (Chimonas, 1993). The waveguide in the Rees et al., 1998 study was bounded by the cold surface and a low-level capping inversion characterized by modest winds, high shear, and a stable atmospheric layer hovering around Ri_c with weaker wind shear above the capping inversion in a near-neutral atmosphere, not unlike the atmospheric properties during VTMX.

Barnard and Riley (2002) used a Direct Numerical Simulation (hereafter referred to as DNS) to model intermittency in a stably stratified fluid. Results obtained from their simulations suggest that, in a thermally stratified state, the atmosphere is susceptible to shear instability leading to overturning eddies and roll vortices forming at the surface. The roll structure lifts cool air from the surface and forces it above the ambient warm air to the height of the local capping inversion. The cold air surrounded by warm air results in short-lived convective instability, creating a locally turbulent environment leading to the formation of structures including plumes, rolls, and eddies. The enhanced mixing in the stratified boundary layer reduces the temperature gradient and decreases the transport of energy from above the capping inversion. The energy dissipates in the waveguide in the absence of additional energy input from

either aloft or from the surface leading to turbulence decay. As the atmosphere returns to its initial stratified state, it once again becomes susceptible to this process. Both results from experiments and simulations (Rees et al., 1998; Sun et al., 2004) point to a similar physical mechanism for the origin of wave propagation and its ensuing turbulence-wave interactions near the surface.

Using lidar data collected in the SBL, a representation of the processes responsible for the transport and exchange of water between the surface and the atmosphere can be obtained both spatially and temporally. The analysis presented here suggests that the initial instability that generated the structures originates above the SBL, from the presence of a local instability, providing the necessary set of conditions required to support various standing pressure or density waves such as K-H waves. These waves propagating to the surface provided certain stability conditions within the atmospheric waveguide (Rees et al., 1998). Finnigan et al. (1984), found that internal gravity waves formed between 550 m and 650 m produced turbulent interactions at the surface. A more detailed study demonstrating the coupling between waves aloft and surface turbulence in the SBL was done by Einaudi and Finnigan (1993). They showed that small pressure perturbations can induce turbulence at the surface.

The evidence for this mechanism in this study comes from both the lidar and point-sensor data including the elastic backscatter image (Fig. 2), the Raman lidar image (Fig. 3), and the vertical wind speed time-series, and the vertical wind speed power spectrum (Fig. 4). The elastic backscatter data shows a wave between 600 and 700 m, with a period of approximately 683 s as estimated by peak power spectrum analysis. Further, the growth and decay of a coherent structure occurs over a 10 scan period equivalent to 540 s. The sonic anemometer w time series spanning 1200 s sampled at 10 Hz shows that this was a substantial decrease in w between 20:31 and 20:32 MST and another large negative fluctuation at 20:43 MST, approximately 696 s after the first episode. Furthermore, the time series also shows at least two potential “ramp” structures of approximately 3.5 to 4 min long. Ramps indicate the passage of coherent structures, such as

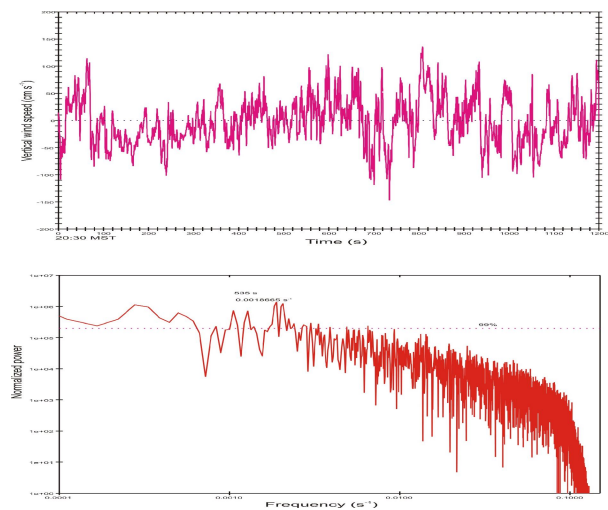


Figure 4. w time series and power spectrum.

eddies and plumes, and have been observed in both the unstable and stable boundary layers (Cooper et al., 1994; Koprov et al., 2004). In addition, a power spectrum shows a peak frequency of $0.00186665 \text{ s}^{-1}$ or a period of 535 s. Independent estimates of the integral time scale from observations of the dissipation rate provided by the scintillometer were also approximately 11 min to 12 min in duration, supporting the contention that a periodic process was occurring. It appears that, given this coincidence of the elevated wave structure period (approximately 11 min.) and similar periods for the surface observed fluctuations in the w time series and dissipation rate, and given the birth and decay of the intermittent structures, the intermittency at the surface of the stable boundary layer is coupled to wave processes aloft.

6. CONCLUSIONS

It appears that under low to modest winds most of the transport between the surface and the atmosphere takes place in the presence of low frequency microscale turbulence. When the gradient Richardson number was between 0 and 0.25 coherent features developed within the first few meters of the surface and were observable with the lidar. These structures tend to be small, with diameters on the order of 20 to 30 m, and were limited in growth by a strong 6 degree thermal capping inversion 20 m thick that developed broadly across the site. Within this inversion shear stresses dominated the development and transport of the intermittent features. The period between the birth and decay of these turbulent events was on the order of 10 minutes. Due to both wind shear and thermal structure of the lower SBL, the structures are most likely the roll vortices predicted by DNS models. These structures appear to be located and defined by a wave guide-like region, which occurs under sub-critical Ri numbers and discontinuities in the scalar profiles. They also appear to be responsible for the containment of the periodic intermittency observed here and in previous studies. The image analysis showed that most of the mass transported vertically during these periods was from these intermittent structures and not by diffusion. In contrast, little structure was identified above the first 20 m; this suggests a more diffusive background.

There are reasonable indications that these microscale structures observed at the surface are coupled to wave properties several hundred meters aloft. At the time of writing, a quantitative mechanism to show this coupling is not available. Independent vertical wind and scintillometer measurements several kilometers downwind of the lidar, showed distinct fluctuations associated with the onset of wave structures at 600 m above ground level. These fluctuations roughly coincide with the microscale turbulence observed by the lidar and are thought to trigger the local instability. During the morning transition period, as soon as the sun heats the air and surface, the SBL decays and the convective ABL forms by a bursting mechanism, with coherent plumes carrying moisture vertically at rates approaching 1 ms^{-1} .

The data presented strongly suggests that the ability to resolve structures between 2 and 20 m scale is important in the SBL. Further, verification of the now-maturing DNS models requires high spatial as well as

temporal data. The unanswered problem then remains: can the modest pressure fluctuations generated by the wave aloft add enough additional energy to the surface to initiate the turbulence observed? The results presented herein, suggest that a dense sub-gridscale network of surface-based remote sensing instruments coupled with multiple fast-response eddy covariance sensors should form part of an intensive study to characterize the underlying physics of SBL intermittency.

7. REFERENCES

- Barnard, J.C. and. Riley, J.J., 2002. Direct numerical simulation of intermittent turbulence in the very stable Ekman layer. Extended abstract No. 9.3, 15th Symp. Boundary Layer and Turbulence, Wageningen, the Netherlands, AMS, Boston, MA 02108. pp 424 - 427.
- Chimonas, G., 1993. Surface drag instabilities in the atmospheric boundary layer. *J. Atmos. Sci.*, 50:1914-1924.
- Chimonas, G., 1999. Steps, waves and turbulence in the stably stratified planetary boundary layer. *Bound.-Layer Meteorol.*, 90:397-421.
- Cooper, D.I., M.Y. Leclerc, J. Archuleta, R. Coulter, W.E. Eichinger, C.Y.J. Kao and C.J. Nappo. Coherent microscale surface structures observed by a scanning lidar and their contribution to mass exchange in the stable boundary layer. *Submitted to Agric. And Forest Meteorol*, Invited paper, 2004
- Cooper, D.I., W.E. Eichinger, J. Archuleta, L. Hipps, J. Kao, M. Y. Leclerc, C. M. Neale, and J. Prueger, 2003. Spatial and temporal footprint analysis of three dimensional moisture fields from lidar, eddy covariance, and a footprint model. *Agric. And Forest Meteorol.* Vol. 114:213–234.
- Cooper, D.I., and W.E. Eichinger, L. Hipps, J. Kao, J. Reisner, S. Smith, S.M. Schaeffer, and Williams, D.G., 2000. Spatial and temporal properties of water vapor and flux over a riparian canopy. *Agric. And Forest Meteorol.*, 105:161-183.
- Cooper, D. I., W. Eichinger, R. Ecke, C.-Y. J. Kao, and Reisner, J. M., 1997. Initial Investigations of micro-scale cellular convection in an equatorial marine atmospheric boundary layer revealed by lidar. *Geophys. Res. Lett.*, 24:45-48.
- Cooper, D. I., W. E. Eichinger, S. Barr, W. Cottingame, M. V. Hynes, C. F. Keller, C. F. Lebeda, and Poling, D. A., 1996. High resolution properties of the equatorial Pacific marine atmospheric boundary layer from lidar and radiosonde observations. *J. Atmos. Sci.*, 53:2054-2075.
- Cooper, D., W. Eichinger, D. Hof, D. Jones, R. Quick, and Tiee, J., 1994. Observations of coherent structures from a scanning lidar. *Agric. and Forest Meteorol.*, 67, 239-252.

- Cooper, D., W. Eichinger, D. Holtkamp, R. Karl Jr., C. Quick, W. Dugas, and Hipps, L., 1992. Spatial variability of water vapor turbulent transfer within the boundary layer. *Bound. Layer Meteorol.*, 61:389-405.
- Cuxart, J., G. Morales, E. Terradellas, and Yagüe, C., 2002. Study of coherent structure and estimation of the pressure transport terms for the nocturnal stable boundary layer. *Bound. Layer Meteorol.*, 105:305-328.
- Doran, C.J., Fast, J.D., and Horel, J., 2002. The VTMX Campaign. *Bull. Amer. Meteorol. Soc.*, 83:537-551.
- Eichinger, W.E. and D.I. Cooper with P.R. Forman, J. Griegos, M.A. Osborn, D. Richter, L.L. Tellier, and Thornton, J., 1998. The development of raman water-vapor and elastic aerosol. Lidars for the central equatorial pacific experiment, *J. of Atmos. and Oceanic Tech.*, 16:1753-1766.
- Eichinger, W., D. Cooper, F. Archuletta, D. Hof, D. Holtkamp, R. Karl Jr., C. Quick, and J. Tiee, 1994. Development and Application of a Scanning, Solar-Blind Water Raman-Lidar. *Applied Optics*, Vol 33, No. 18 3923- 3932.
- Einaudi, F. and Finnigan, J. J., 1981. The interaction between an internal gravity wave and the planetary boundary layer. *Quart. J. Roy. Metero. Soc.*, 107, 793-806.
- Einaudi, F. and Finnigan, J. J., 1993. Wave-turbulence dynamics in the stably stratified boundary layer. *J. Atmos. Sci.*, 50, 1841-1864.
- Finnigan, J. J., 1988. Kinetic energy transfer between internal gravity waves and turbulence. *J. Atmos. Sci.*, 45, 486-505.
- Finnigan, J. J. and Einaudi, F., 1981. The interaction of an internal gravity wave and the planetary boundary layer. II: Effects of the wave on the turbulence structure. *Quart. J. Roy. Metero. Soc.*, 107, 807-832.
- Finnigan, J.J. F. Einaudi, and Fua, D., 1984. The interaction between an internal gravity wave and turbulence in the stably-stratified nocturnal boundary layer. *J. of Atmos. Sci.*, 41:2409-2436.
- Kao, C.-Y. J., D.I. Cooper, J. M. Reisner, W. E. Eichinger, M. Ghil, 2002 Probing atmospheric turbulence with high-resolution lidar and models. *JGR-Atmos.* Vol 107, D9:7.1-7.10.
- Koprov, B.M., V.M. Koprov, T.L. Makarova, and Golitsyn, G.S., 2004. Coherent structures in the atmospheric surface layer under stable and unstable conditions. *Bound. Layer Meteorol.*, 111:19-32.
- Mahrt, L., and Vickers, D., 2002. Contrasting vertical structures of nocturnal boundary layers. *Bound. Layer Meteorol.*, 105:351-363.
- Mahrt, L., 1999. Stratified atmospheric boundary layers. *Bound. Layer Meteorol.*, 90:375-396.
- Rees, J. A., P.S. Anderson and King, J.C., 1998. Observations of solitary waves in the stable atmospheric boundary layer. *Bound. Layer Meteorol.*, 86:47-61.
- Staquet, C., and Sommeria, J., 2002. Internal gravity waves: from instabilities to turbulence. *Annu. Rev. Fluid Mech.*, 34:559-593.
- Sun, J., D. Lenschow, S.P. Burns, R.M. Banta, R.K. Newsom, R.F. Coulter, I.T. Stephens, C. Nappo, B. Balsley, M. Jensen, L. Mahrt, D. Miller, and Skelly, B., 2004. Atmospheric disturbances that generate intermittent turbulence in nocturnal boundary layers. *Bound. Layer Meteorol.*, 110: 255-279.

8. ACKNOWLEDGMENTS

We would like to thank A. Fernandez, K. Vigil, and A. Reeves of LANL for their time and effort. We would also like to thank D. Whiteman of PNNL and his associates for their technical and logistical support in running the tethersondes and compiling the data. We also thank the staff of the Salt Lake City Utilities Department for allowing us to work on their site. In addition, we would like to thank C. Doran of PNNL and R. Petty and P. Lunn of DOE-OBER for their time and effort to make VTMX possible. This work was performed and funded in part under DOE grant W7405-ENG-36.